ISSN 1063-7834, Physics of the Solid State, 2015, Vol. 57, No. 4, pp. 659–674. © Pleiades Publishing, Ltd., 2015.
Original Russian Text © Sh.A. Mirsagatov, I.B. Sapaev, 2015, published in Fizika Tverdogo Tela, 2015, Vol. 57, No. 4, pp. 646–660.

SEMICONDUCTORS

Mechanism of Charge Transfer in Injection Photodetectors Based on the *M*(In)–*n*-CdS–*p*-Si–*M*(In) Structure

Sh. A. Mirsagatov* and I. B. Sapaev

Physical-Technical Institute, Scientific and Production Association "Physics–Sun," Academy of Sciences of Uzbekistan, ul. G. Mavlyanova 2B, Tashkent, 700084 Uzbekistan

** e-mail: mirsagatov@uzsci.net, mohim@inbox.ru*

Received September 16, 2014; in final form, November 12, 2014

Abstract—The mechanism of charge transfer in a new-type selective (with a tunable spectrum) injection photodetector based on the *M*(In)–*n*-CdS–*p*-Si–*M*(In) structure with the internal amplification has been analyzed. It has been shown that, in this structure, there is a mutual compensation of the drift and diffusion fluxes of charge carriers. The counter drift and diffusion fluxes of nonequilibrium carriers at reverse current densities $I \sim 10^{-8}$–10^{-7} A/cm^2 lead to the appearance of sign-reversal points of the photosensitivity in the short-wavelength and long-wavelength regions of the spectrum. The mutual compensation of the counter drift and diffusion current fluxes at current densities of the order of $\sim 10^{-6}$ A/cm^2 leads to the appearance of a sublinear section in the reverse current–voltage characteristic over a wide range of bias voltages. It has been found that the *n*-SdS–*p*-Si heterojunction has a low density of surface states at the interface. This makes it possible to develop an injection photodetector based on the considered structure with a high spectral sensitivity $S_\lambda = 5.0 \times 10^4$ A/W) and a high integrated sensitivity $S_{\text{int}} = 2.8 \times 10^4$ A/lm or 4.5×10^6 A/W in the forward direction of the current.

DOI: 10.1134/S1063783415040162

1. INTRODUCTION

In the literature, there is no information on the development of selective photodetectors with the internal amplification, which are tunable at desired electromagnetic radiation wavelengths under external influences (for example, at an applied bias voltage) and can selectively detect electromagnetic radiation. The fabrication of these devices is an important problem, because one selective photodetector replaces several photodetectors that are sensitive to different ranges of electromagnetic radiation wavelengths and are closely related to the band gap. In our view, such a multifunctional photodetector can be developed based on a semiconductor structure with heterojunctions and controlled counter current fluxes of nonequilibrium charge carriers. Owing to this control, there is a sign reversal of the photosensitivity at different thicknesses of the base, which correspond to specific electromagnetic radiation wavelengths in the wavelength range of 300–1200 μm. In this case, if the base of the structure has a high electrical resistivity and is dominated by diffusion currents in the current transport, the photodetector, in addition to the above properties, also exhibits the property of internal amplification of the primary photocurrent. Elements of this structure should consist of semiconductors that are sensitive to optical signals in the near-ultraviolet, visible, and near-infrared regions of the electromagnetic radiation spectrum.

Such selective injection photodetector with high output parameters can be developed based on the *M*(In)–*n*-CdS–*p*-Si–*M*(In) structure with a heterojunction.

The literature contains information about the design and fabrication of injection photodiodes based on II–VI compounds, in particular, based on cadmium sulfide and cadmium telluride and their solid solutions [1–4]. Koldaev et al. [1] considered the Ni–*n*-CdS–n^+-CdS structure based on CdS single crystals, in which the amplification of the photocurrent occurs under illumination with light at a wavelength $\lambda = 0.22$ μm with the injection of majority charge carriers into the high-resistivity *n*-region on the unilluminated side of the n^+–*n* junction.

In the *M*(In)–*n*-CdS–*p*-Si–*M*(In) structure proposed in our work, the high-resistivity highly compensated CdS layer with a low *n*-type conductivity plays the role of an *i*-layer. The choice of the *n*-CdS–*p*-Si heterojunction was motivated by the fact that this heterojunction was described in the literature [5]. Moreover, silicon is a well-studied material. In the structure under consideration, the *n*-CdS–*p*-Si heterojunction occupies a special place, because its parameters determine, to a large extent, the electrophysical and photoelectric properties, and, finally, the mechanism of charge carrier transfer in the structure. It is known that the lattice constants and thermal expansion coefficients of cadmium sulfide and silicon differ signifi-

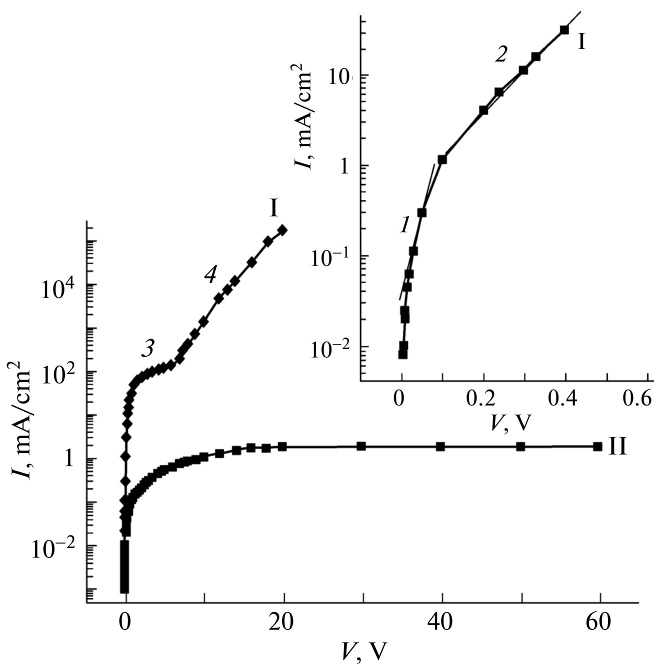

Fig. 1. Current–voltage characteristic of the structure on a semilogarithmic scale in the dark: (I) forward branch with (*3*) third and (*4*) fourth sections and (II) reverse branch with (*1*) first and (*2*) second sections (shown in the inset).

cantly from each other. Consequently, the density of surface states at the interface of the heterojunction can be significant. Therefore, special attention should be paid to the methods used for decreasing the density of surface states at the interface between cadmium sulfide and silicon. In order to solve this problem, it is necessary to use different factors, such as the significant ionic bond in CdS and the presence of a SiO_2 film with a thickness of ~20 Å ("dead" layer) [6] on the silicon surface, which can affect the decrease in the density of surface states generated at the interface of the *n*-CdS–*p*-Si heterojunction. The purpose of this work was to investigate the mechanism of charge carrier transfer in the *M*(In)–*n*-CdS–*p*-Si–*M*(In) structure, both in the dark and in the light, in order to answer the question as to how effectively this structure operates and how much its properties correspond to the multifunctional properties of the photodetector.

2. SAMPLE PREPARATION AND EXPERIMENTAL TECHNIQUE

For our investigations, the photosensitive *M*(In)–*n*-CdS–*p*-Si–*M*(In) structure was prepared by deposition of CdS powders (in a quasi-closed system under a vacuum of 10^{-5} Torr) onto the surface of a *p*-type silicon wafer with an electrical resistivity $\rho \approx 10\ \Omega$ cm and a thickness of 300 μm [7]. The source (CdS) had a temperature $T_{source} \approx 800–850°C$, and the temperature of the substrate (*p*-Si) was maintained within the range $T_s \approx 250–270°C$. The investigations performed with an MII-4 microscope revealed that the CdS films grown on the *p*-Si-substrate consist of columnar crystallites (grains), which are oriented in the direction of the film growth and azimuthally misoriented. It was found that the crystallite size depends substantially on the technological conditions, primarily on the temperature T_s of the silicon substrate. For example, crystallites in the CdS films grown at the substrate temperature $T_s = 300°C$ had a size of ~3–4 μm and totally penetrated throughout the entire film with a thickness $w \approx 2$ μm. The grown CdS films had a high electrical resistivity $\rho \approx (2–3) \times 10^{10}\ \Omega$ cm and a low *n*-type conductivity. Further, the metal–semiconductor contact was prepared by deposition of indium onto the surface of the CdS film under a vacuum of 10^{-5} Torr for 25–30 s at a substrate temperature of 373 K.

The Π-shaped ohmic contacts were also deposited by means of the vacuum evaporation of indium.

The current–voltage (*I*–*V*) characteristics of the fabricated *M*(In)–*n*-CdS–*p*-Si–*M*(In) structures were measured in the forward and reverse directions of the current in the dark and in the light at the illuminance $E = 0.1–100$ lx at room temperature. The structures were illuminated with white light from an LG-75 laser at a radiation power in the range from 10 μW/cm² to 0.75 mW/cm² with a wavelength of 0.625 μm, as well as using an incandescent lamp with the parameters approximately corresponding to a reference lamp. For this lamp, one lumen (1 lm) of electromagnetic radiation in the visible spectral region contains 9.1×10^{-3} W [8]. The spectral dependence of the photosensitivity of the structures was measured on a 3MR-3 monochromator at a temperature $T = 300$ K. The radiation source was a DKSSh-1000 xenon lamp operating in the mode of the minimum allowable power. The lamp provided a light flux of 53000 lm and a brightness of 120 Mcd/m² in the center of the light spot. The radiation power of the lamp was calibrated in absolute units with the use of a thermoelement equipped with an RTE-9 quartz window. The DKSSh-1000 xenon lamp in the ultraviolet and visible regions had a continuous spectrum.

3. EXPERIMENTAL RESULTS AND DISCUSSION

The forward and reverse branches of the current–voltage characteristic of a typical *M*(In)–*n*-CdS–*p*-Si–*M*(In) structure are plotted on a semilogarithmic scale in Fig. 1. The forward and reverse directions of the current in the structure were provided by applying the negative and positive potentials to the *p*-Si contact, respectively. The analysis of the current–voltage characteristics demonstrated that the studied structure exhibit rectifying properties with a rectification ratio $K \sim 10^5$ (the quantity *K* is determined as the ratio of the forward and reverse currents at a fixed voltage of 25 V).

3.1. Spectral Distribution of the Photosensitivity

The spectral distributions of photosensitivity S_λ without and with applying the bias voltage V in the forward and reverse directions of the current are shown in Figs. 2a and 2b. The analysis of the spectral distribution of photosensitivity in the forward direction of the current shows (Fig. 2a) that this curve has the spectral range $\lambda = 389–1238$ nm. The spectral sensitivity of this structure begins with the wavelength $\lambda = 389$ nm, rapidly increases, and reaches the maximum value $S_\lambda = 2.7$ A/W at the wavelength $\lambda = 480$ nm in the absence of a bias voltage. Then, the spectral sensitivity decreases to zero at $\lambda = 872.7$ nm. The photosensitivity decay curve has a number of specific features, which manifest themselves in the form of a step at $\lambda = 541.84–578.56$ nm and three small peaks at $\lambda = 618$, 740, and 821.8 nm. These features are associated with the presence of impurities in cadmium sulfide layers.

Next (after the zero value at $\lambda = 872.7$ nm), the spectral sensitivity reveres sign, begins to increase, and at $\lambda = 961.8$ nm reaches the maximum value $S_\lambda \sim 0.2$ A/W. Then, the spectral sensitivity smoothly decreases to zero with an increase in the wavelength λ ($\lambda = 1042.8$ nm), after which it again increases (with a sign reversal) and at $\lambda = 1200.3$ nm, the value of S_λ reaches the maximum of ~0.93 A/W. Further, with an increase in the electromagnetic radiation wavelength, the spectral sensitivity begins to decrease.

After applying a bias voltage to the sample, the shape of the dependence $S_\lambda(\lambda)$ remains unchanged, and only the spectral sensitivity increases in magnitude, especially at the wavelengths $\lambda_1 = 480$ nm and $\lambda_2 = 872.7$ nm, which correspond to peaks in the spectral dependence of S_λ. For example, $S_\lambda = 2.7$ A/W at $V = 0$ V and $S_\lambda = 4.1$ A/W at $V = 2$ mV. A similar pattern can be observed for the second peak ($\lambda = 961.8$ nm), for which $S_\lambda = 0.9$ A/W at $V = 0$ V and $S_\lambda = 1.37$ A/W at $V = 2$ mV. These data demonstrate that the M(In)–n-CdS barrier and the n-CdS–p-Si heterojunction effectively separate the generated electron–hole pairs, and the internal amplification occurs in the structure. In this case, in the greater part of the spectral range of the photosensitivity, the value of S_λ significantly exceeds the spectral sensitivity of the ideal photodetector (Fig. 2a, curve *4*). The ideal photodetector is a photodetector in which all the incident photons are absorbed and generate electron–hole pairs that are separated without loss by a potential barrier and contribute to the photocurrent. In principle, such a photodetector cannot be created. Nevertheless, the experimental values of the spectral sensitivity over a wide spectral range significantly exceed the values of S_λ for the ideal photodetector at a given electromagnetic radiation wavelength. This indicates the internal amplification; moreover, the studied structure is very sensitive to small levels of illumination. The high values of the integrated and spectral sensitivities are observed both in the intrinsic and impurity absorption regions.

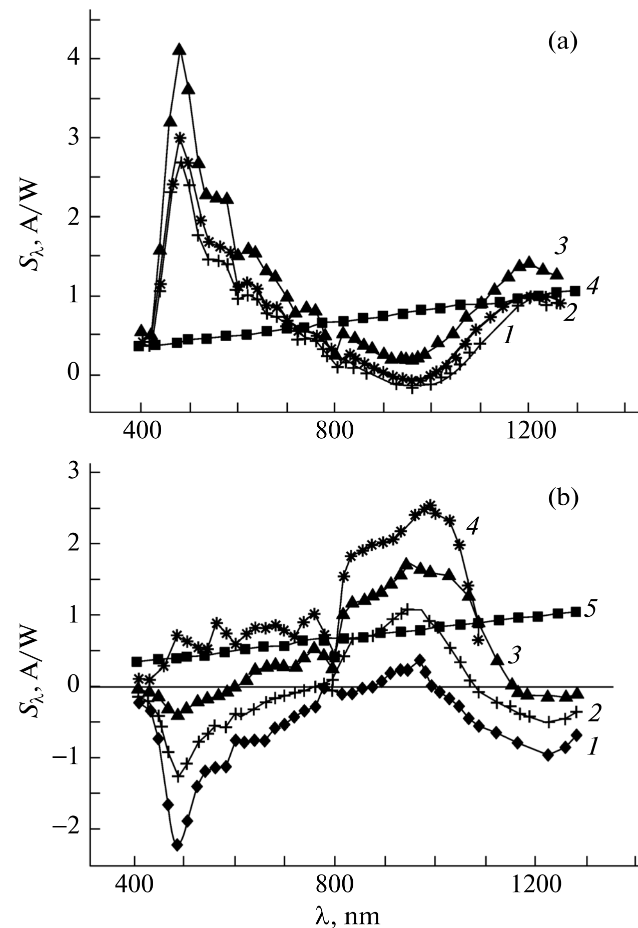

Fig. 2. (a) (*1–3*) Spectral dependences of the photosensitivity of the M(In)–n-CdS–p-Si–M(In) structure (*1*) in the absence of bias voltage and (*2*, *3*) at applied bias voltages $V =$ (*2*) 0.5 and (*3*) 2.0 mV in the forward direction of the current. (*4*) Spectral dependence constructed for an ideal photodetector according to the formula $S_\lambda = \frac{e}{hc}\lambda\eta_\lambda$. (b) (*1–4*) Spectral dependences of the photosensitivity of the M(In)–n-CdS–p-Si–M(In) structure (*1*) in the absence of bias voltage and (*2–4*) at applied bias voltages $V =$ (*2*) 4, (*3*) 6, and (*4*) 8.5 mV in the reverse direction of the current. (*5*) Spectral dependence constructed for an ideal photodetector according to the same formula as for curve *4* in panel (a).

Now, we consider the spectral sensitivity as a function of the wavelength in the reverse direction of the current in the absence and in the presence of different bias voltages (Fig. 2b). It can be seen from this figure (curve *1*) that, in the absence of a bias voltage, the spectral sensitivity range lies in the wavelength range $\lambda = 350–1350$ nm and the parameter S_λ has the highest absolute values at $\lambda_1 \approx 480$ nm and $\lambda_2 \approx 1248$ nm, where the photocurrent has a negative value. In the short-wavelength region, with an increase in the electromagnetic radiation wavelength, the spectral sensi-

tivity S_λ decreases in the absolute value and, at $\lambda \approx$ 865.45 nm, becomes equal to zero, then changes the sign, and begins to increase with a further increase in the value of λ. In the long-wavelength region, the peak in the dependence $S_\lambda(\lambda)$ is observed at $\lambda \approx 949.5$ nm in the range of positive photocurrents. Further, the spectral sensitivity S_λ decreases again and passes through zero at $\lambda \approx 1000$ nm; then the photosensitivity changes the sign and increases sharply in magnitude up to $\lambda \approx$ 1130 nm. With a further increase in the electromagnetic radiation wavelength, the photosensitivity decreases again. After applying a bias voltage, the sign-reversal point of the photocurrent in the short-wavelength region of the spectrum is significantly shifted toward shorter wavelengths, and the absolute value of the photocurrent decreases with an increase in the bias voltage (Fig. 2b). A similar behavior of the photocurrent in the dependence $S_\lambda(\lambda)$ is observed in the long-wavelength region of photosensitivity. However, in this case, the sign-reversal point of the photocurrent is shifted toward longer wavelengths of electromagnetic radiation. Moreover, the rate of change in the absolute value of the photocurrent as a function of the bias voltage is significantly less than that in the short-wavelength region of the spectrum. For example, the sign-reversal point of the photocurrent is shifted by ~260 nm at an applied bias voltage $V = 6$ mV in the short-wavelength region of the spectrum, whereas in the long-wavelength region of the spectrum, it is shifted by only 168 nm. The experiment demonstrates that, when the bias voltage applied to the structure is equal to 8.5 mV, the dependence $S_\lambda(\lambda)$ entirely covers the region of positive photocurrents (Fig. 2b, curve *4*). This behavior of the dependence $S_\lambda(\lambda)$ of the reverse-biased *M*(In)–*n*-CdS–*p*-Si–*M*(In) structure is explained as follows. First, the *M*(In)–*n*-CdS junction and the *n*-CdS–*p*-Si heterojunction effectively separate light-generated nonequilibrium electron–hole pairs. Second, the *n*-CdS–*p*-Si heterojunction injects electrons into the base (*n*-CdS) of the structure at an applied reverse bias voltage. Third, in the base of the structure under investigation, the bipolar diffusion current increases in magnitude with an increase in the applied reverse bias voltage. In the reverse-biased *M*(In)–*n*-CdS–*p*-Si–*M*(In) structure, electrons are injected from the *p*-Si layer into a high-resistivity compensated *n*-CdS layer at a sufficient concentration of electrons in the *p*-Si layer or, when the thickness of this layer is comparable to the diffusion length. In the silicon substrate, the concentrations of equilibrium holes and electrons are equal to 1.3×10^{15} and 7.7×10^4 cm^{-3}, respectively, for the electron mobility $\mu_n =$ 1500 cm^2/(V s), the hole mobility $\mu_p = 480$ cm^2/(V s), and the intrinsic carrier concentration $n_i = 10^{10}$ cm^{-3}. Hence, it follows that the concentration of nonequilibrium electrons in the *p*-Si substrate is approximately the same as the concentration of electrons ($n_0 \approx$ 10^5 cm^{-3}) in the base (*n*-CdS layer), which was determined for the parameters $\rho_{CdS} \approx 3 \times 10^{10}$ Ω cm and $\mu_n = 100$ cm^2/(V s) [9]. Moreover, we should take into account the probability of injection of electrons from the metal contact (In) deposited on *p*-Si, because the thickness of the silicon wafer is of the same order of magnitude with the electron diffusion length L_n, which is ~400 μm for the parameters $\tau_n \approx 50$ μs and $\mu_n = 1500$ cm^2/(V s) [10].

The appearance of a peak in the photosensitivity curve with the maximum at the wavelength $\lambda = 947$ nm suggests that the space charge of the *n*-CdS–*p*-Si heterojunction effectively injects nonequilibrium holes, which are generated in the base, into the *p*-Si layer.

An increase in the photocurrent in the peak and its broadening toward shorter wavelengths with the applied bias voltage indicates that, in the base of the structure, the bipolar diffusion current of nonequilibrium minority carriers (holes), which are supplied to ensure the electrical neutrality of the injected electrons from the *n*-CdS–*p*-Si heterojunction, increases with an increase in the bias voltage. Since the structure under investigation has a high-resistivity base, nonequilibrium charge carriers, whose direction coincides with the direction of the diffusion of hole minority carriers [11], diffuse in the form of a plasma; i.e., electron–hole pairs move together.

The appearance of a sign-reversal point in the dependence of the spectral distribution of the photocurrent gives reason to believe that the oppositely directed diffusion and drift current fluxes in the base of the structure completely compensate each other at a specific thickness of the base. This thickness of the base corresponds to the depth of the absorption of electromagnetic radiation with a wavelength λ. The shift of the sign-reversal point of the photosensitivity toward shorter wavelengths is determined by the bipolar diffusion current, which is associated with the injection of electrons from the *n*-CdS–*p*-Si heterojunction into the base. The shift of this point occurs by means of applying small reverse bias voltages. The experiment demonstrates that, after applying the bias voltage $V \geq 8.5$ mV, the bipolar diffusion current in the structure becomes dominant. Therefore, in the spectrum of the photosensitivity distribution, the sign-reversal point of the photocurrent does not appear.

The analysis of the spectral sensitivity of the peak in the long-wavelength region shows that, in the *p*-Si substrate, there are electrons injected from the ohmic contact (In), which create diffusion and drift electron fluxes directed toward the *n*-CdS–*p*-Si heterojunction. In addition, there arise diffusion fluxes of nonequilibrium electrons directed from the heterojunction to the metal contact due to the accumulation of electrons near the heterojunction. The shift of the sign-reversal point of the photosensitivity in the long-wavelength region of the spectrum toward longer wavelengths shows that the diffusion current directed toward the drift and diffusion fluxes of electrons from

the metal contact increases with an increase in the bias voltage [12, 13]. This situation occurs when the concentration and gradient of electrons at the heterojunction become greater than those in the vicinity of the metal contact (In). This effect is observed when the n-CdS–p-Si heterojunction has a potential barrier and skips not all electrons coming from the opposite indium contacts. The shift in the long-wavelength region of the spectrum at the bias voltage $V = 8.5$ mV becomes smaller than that at $V = 6$ mV. This demonstrates that the n-CdS–p-Si heterojunction begins to skip electrons; i.e., the accumulation of electrons becomes weaker due to changes in the properties of the heterojunction.

The above analysis of the spectral distribution of the photosensitivity in the reverse direction current confirms that electrons from the n-CdS–p-Si heterojunction are injected into the base.

Further, in order to prove the existence of the primary photocurrent amplification, we investigated the dark and light current–voltage characteristics of the structure (Fig. 3). The light current–voltage characteristics were measured at different levels of illumination E by the white light and at different powers P of laser irradiation with the wavelength $\lambda = 625$ nm (Table 1). The performed investigations demonstrate that there is indeed a photocurrent enhancement effect in the M(In)–n-CdS–p-Si–M(In) structure. For example, we have the spectral sensitivity $S_\lambda = 2.3 \times 10^4$ A/W under irradiation from a laser with the power $P = 10$ μW/cm^2 and the integrated sensitivity $S_{int} = 2.75 \times 10^4$ A/lm (3×10^6 A/W) under irradiation by the white light with the illuminance $E = 0.1$ lx at room temperature and at a bias voltage $V = 20$ V (Table 1). It should be noted that the structure under investigation is very sensitive to small levels of illumination and has

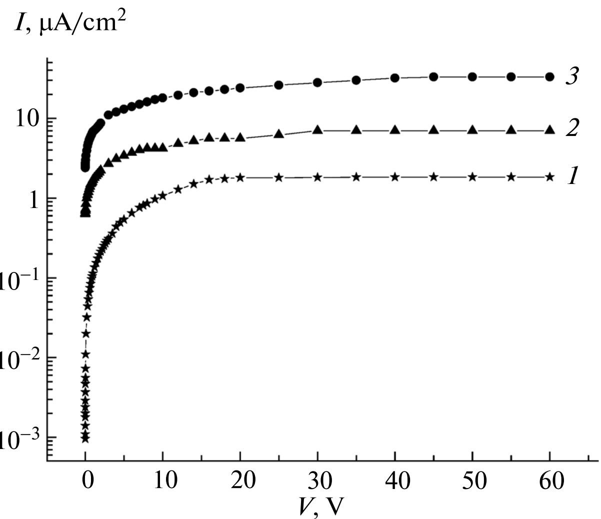

Fig. 3. Dark and light current–voltage characteristics of the reverse branch: (*1*) in the dark, (*2*) under irradiation by white light with the illuminance $E = 0.1$ lx, (*3*) under laser irradiation with a wavelength $\lambda = 625$ nm and a laser power $P = 10$ μW/cm^2.

Table 1. Photocurrent I_{Ph}, integrated sensitivity S_{int}, and spectral sensitivity S_λ of the structure as functions of the illuminance E, laser irradiation power P, and bias voltage V

White light					Laser irradiation		
E, lx	V, V	I_{Ph}, μA/cm^2	S_{int}, A/lm	S_{int}, A/W	P, μW/cm^2	I_{Ph}, μA/cm^2	S_λ, A/W
0.05	5	120	24	0.26×10^4	0.7	25	36
	10	1920	384	4.2×10^4		385	550
	15	14614	2923	3.21×10^5		2140	3057
	20	203250	40650	4.47×10^6		35250	50358
0.1	5	148.6	14.8	0.2×10^4	10	133	13.3
	10	2354.4	235.44	2.6×10^4		2000	200
	15	17000	1700	1.87×10^5		11200	1120
	20	274500	27450	3×10^6		233560	23356
1	5	178	1.78	0.2×10^3	50	369.2	7.4
	10	3020	30.2	3.32×10^3		6075.6	121.5
	15	18000	180	1.98×10^4		38937.1	778.7
	20	310220	3102	3.4×10^5		416333	8326
10	5	184	0.184	0.2×10^2	100	456	4.56
	10	3600	3.6	4×10^2		7524	75.24
	15	21000	21	2.31×10^3		44025	440.25
	20	410500	410	4.5×10^4		448320	4483.2

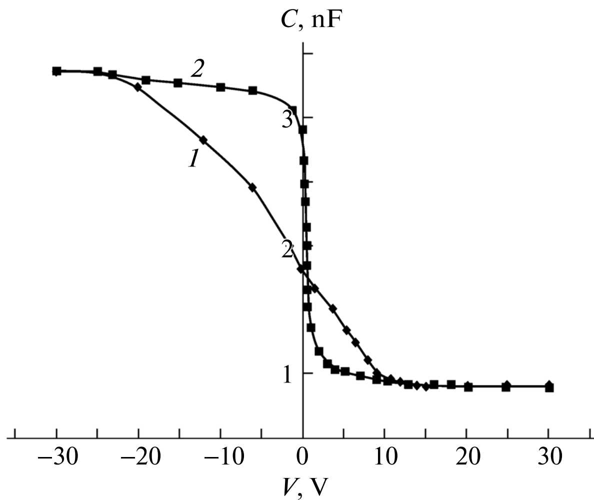

Fig. 4. Capacitance–voltage characteristic of the M(In)–n-CdS–p-Si–M(In) structure at a frequency $f = 10$ kHz and a temperature $T = 300$ K.

high values of the integrated and spectral sensitivities in the intrinsic and impurity absorption regions (Table 1). Moreover, it was found that an increase in the level of illumination by the white light and an increase in the laser irradiation power lead to a decrease in the integrated sensitivity S_{int} and the spectral sensitivity S_λ, whereas an increase in the forward bias voltage leads to an increase in the spectral and integrated sensitivities.

In the structure under investigation, the transfer of charge carriers is determined in many aspects by the properties of the n-CdS–p-Si heterojunction. Therefore, before analyzing the current–voltage characteristics, we investigate the capacitance–voltage characteristics of the structure.

3.2. Capacitance–Voltage Characteristic

One of the informative and nondestructive methods used for obtaining information about the interface is the method of frequency capacitance–voltage characteristics. According to the analysis of the capacitance–voltage characteristics of the structure under investigation, we are dealing here with the metal–insulator–semiconductor (MIS) structure) (Fig. 4). This is quite natural because, in the M(In)–n-CdS–p-Si–M(In) structure, the n-CdS layer is a high-resistivity compensated material. Therefore, this layer and oxide layers formed during the deposition of CdS on the surface of a silicon wafer under vacuum can manifest themselves as an insulator. The experimental capacitance–voltage characteristic (Fig. 4, curve *1*) was measured at room temperature at a frequency of the test signal $f = 10$ kHz, because, at the given frequency, the capacitance–voltage characteristic of the MIS structure is more clearly pronounced. This means that the densities of surface states N_{SS} in the heterojunction are slow surface states.

Using the capacitance of the insulator $C_i = 3.35$ nF and the formula for the parallel-plate capacitor $C = \varepsilon_0\varepsilon S/d$, we determined the thickness of the insulator $d_i \sim 0.26$ μm at the parameters $\varepsilon_0 = 8.85 \times 10^{-14}$ F/cm, $\varepsilon = 10$, and $S \approx 0.1$ cm^2. The calculated thickness of the insulator differs from the thickness of the high-resistivity base (n-CdS), which is equal to ~2 μm. From the minimum capacitance of the structure $C_{min} \approx 0.9$ nF (Fig. 4), we determined the thickness of the space charge $W \approx 0.98$ μm [14], which is approximately equal to half the thickness of the base (n-CdS). At thermodynamic equilibrium, the thickness of the space charge, which was calculated from the capacitance $C = 1.8$ nF in the absence of a bias voltage, was found to be ~0.49 μm. These results are logical if we take into account that the thickness of the space charge decreases in the forward direction of the current and, on the contrary, increases in the reverse direction of the current as the bias voltage increases. Moreover, these experimental data also suggests that the resistance of the space charge is a determining resistance of the structure as a whole. This is indicated by the fact that the capacitance of the space charge coincides with the capacitance of the insulator in the capacitance–voltage characteristic. The appearance of a plateau in the capacitance–voltage characteristic after applying the reverse bias voltage $V = 25$–30 V is explained by the fact that the expansion of the space charge is compensated by the injection of electrons from the n-CdS–p-Si heterojunction.

The density of surface states of the MIS structure is determined from the shift in the experimental capacitance–voltage characteristic with respect to the calculated curve at the same capacitance [14]. Hence, it follows that $N_{SS} = \Delta VC/q$.

For the calculated capacitance–voltage characteristic, the concentration of equilibrium holes p_0 was determined from the flat band capacitance and from the circular section of the capacitance–voltage characteristic. In order to determine the concentration of equilibrium holes p_0 from the capacitance–voltage characteristic, the steep section of this characteristic was plotted in the C^{-2}–V coordinates, in which it has two slopes (Fig. 5, straight lines *1* and *2*). From the slopes of these straight lines, according to the standard formula [15]

$$p_0 = \frac{2}{q\varepsilon_0\varepsilon_S S^2}\frac{dV}{d(C^{-2})}, \tag{1}$$

where q is the electron charge, ε_0 is the dielectric constant of free space, ε_S is the dielectric permittivity of the semiconductor, V_D is the potential barrier height, and S is the surface area of the structure, we determined the concentrations of equilibrium holes p_0 =

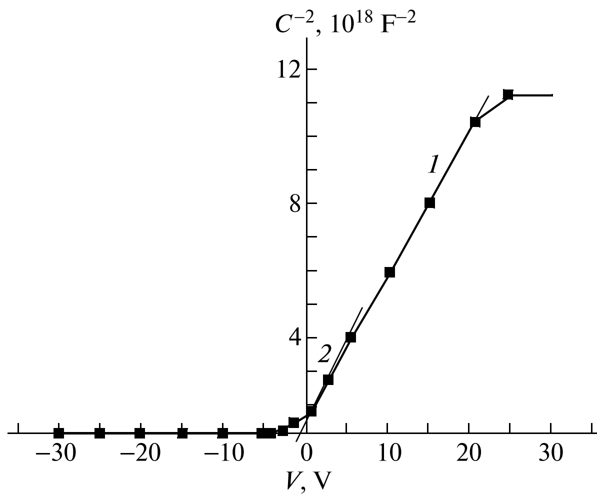

Fig. 5. Capacitance–voltage characteristic of the M(In)–n-CdS–p-Si–M(In) structure in the C^{-2}–V coordinates at a frequency f = 10 kHz and a temperature T = 300 K.

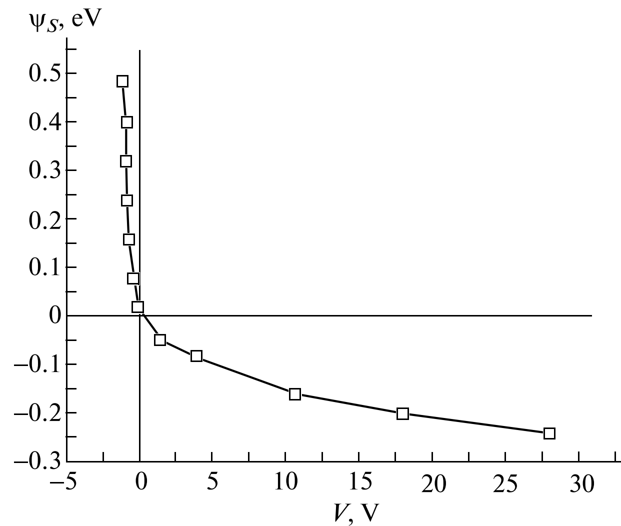

Fig. 6. Dependence of the surface potential of the applied bias voltage.

8.3×10^{14} and 2.1×10^{15} cm^{-3}, respectively. This means that the subsurface semiconductor–silicon layer is nonuniform in thickness. By extrapolating the dependence $C^{-2}(V)$ on the voltage axis V, we determined the height of the potential barrier $V_D = 0.89 \pm 0.02$ eV for electrons of the metal into p-Si. The concentration of equilibrium holes was also determined from the flat band capacitance according to the formula [14]

$$C_{\rm pz} = \frac{\varepsilon_0 \varepsilon_i S}{d_i + \frac{\varepsilon_i}{\varepsilon_S}\sqrt{\frac{kT\varepsilon_0\varepsilon_i}{p_0 q^2}}}, \quad (2)$$

where ε_i is the permittivity of the insulator and d_i is the thickness of the insulator. In this case, it was found that $p_0 \approx 1.8 \times 10^{15}$ cm^{-3}.

The concentrations of equilibrium holes p_0 determined from the capacitance–voltage characteristic are in good agreement with the equilibrium hole concentration ~1.3×10^{15} cm^{-3} obtained for p-Si.

The calculated capacitance–voltage characteristic (Fig. 4, curve *2*) was constructed in the same manner as in [14].

The dependence of the surface potential ψ_S determined as in [16] on the applied bias voltage is shown in Fig. 6. The dependence of N_{SS} on ψ_S is shown in Fig. 7.

The analysis of the dependence ψ_S (V) demonstrates that, at thermodynamic equilibrium, the structure has the surface potential $\psi_S = 0.04$ eV. This means that, at the interface, the surface of a semiconductor (silicon) is negatively charged, which leads to a downward band bending. The downward band bending can also occur due to the presence of negatively charged acceptor surface states that capture holes from the valence band and transform into the neutral state, which results in the formation of a depletion layer on the surface of p-Si. It can also be seen from the figure that the flat band state is realized when the positive bias voltage V = 1.68 V is applied to the top M(In) electrode, after which a further increase in the bias voltage leads to the upward band bending. After applying a negative potential to the M(In)–n-CdS contact, the structure under investigation is turned up in the forward direction of the current; therefore, electrons are injected from the n-CdS layer into p-Si, but no injection of holes from silicon into n-CdS occurs [17]. Let us assume for simplicity that the effective masses and other parameters of the charge carriers are equal to each other, respectively. Hence, we can write the

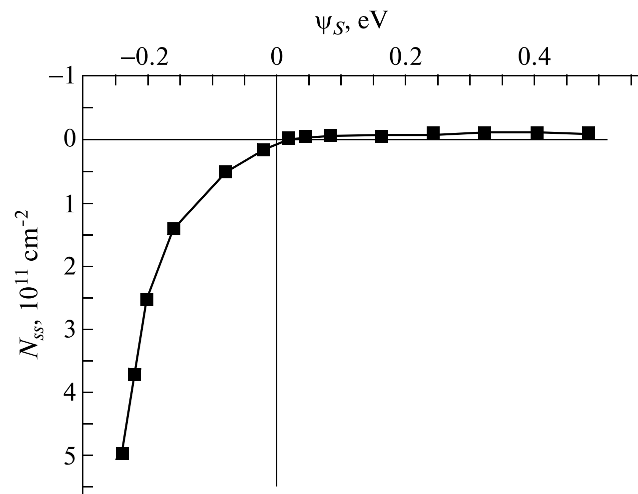

Fig. 7. Dependence of the effective density of surface states on the surface potential.

expression $M = (I_p/I_n) = \exp[-(E_{gn} - E_{gp})/kT]$ [17], where E_{gn} and E_{gp} are the band gaps of the wide-band-gap and narrow-band-gap semiconductors, respectively; and I_p and I_n are the currents of holes and electrons, respectively. The quantity M shows that the current flows from the wide-band-gap semiconductor into the narrow-band-gap semiconductor. Indeed, from the relationship for M. it follows that the ratio M is the more rigorous, the greater is the difference between the band gaps ΔE_g of the semiconductors. For example, in the case of the heterojunction between silicon and germanium, the ratio between the currents flowing from silicon into germanium and the currents flowing from germanium into silicon differs by a factor of e^{-16}. In our case, the difference between the band gaps ΔE_g of Si and CdS forming the heterojunction is equal to 1.3 eV, whereas for Si and Ge, we have ΔE_g = 0.4 eV. Hence, it follows that the ratio M for the n-CdS–p-Si heterojunction should be significantly greater, and the current flowing in the structure under investigation is determined exclusively by electron beams from n-CdS into p-Si. The above arguments are valid for ideal heterojunctions. In real heterojunctions, surface states exist at the interface between the semiconductors, and, therefore, the ratio M may be not strict. Surface states are formed according to the following reasons: (a) due to the difference in the crystal lattice constants of p-Si and n-CdS contacting with each other, which is more than 7% [6]; and (b) during the technological processes. These surface states can be recombination centers or centers of tunneling for holes into the base of the structure. Nevertheless, we assume that the current flowing in the structure is predominantly determined by electron fluxes coming from the M(In)–n-CdS junction. Therefore, there occurs a downward band bending. Furthermore, it was found that the surface potential changes significantly with an increase in the bias voltage. For example, when the bias voltage $V = -1.12$ V is applied to the top metal electrode, the surface potential becomes equal to 0.48 eV. However, when the positive reverse bias voltage is applied to the top metal electrode, the surface potential $\psi_S(V)$ varies relatively little. For example, at the applied bias voltage $V = 27$ V, the surface potential ψ_S is bent upward by only –0.24 eV. This behavior of the surface potential is caused by a high density of surface states in the upper half of the band gap of silicon. This assumption is confirmed by the performed experimental investigations of the distribution of surface states N_{SS} as a function of the surface potential ψ_{SS} (Fig. 7). The dependence $N_{SS}(\psi_S)$ is characterized by a higher density of surface states at positive values of the surface potential, and the value of N_{SS} becomes equal to $\sim 6 \times 10^{11}$ cm^{-2} at $\Psi_S = -0.24$ eV. The value of N_{SS} in the lower half of the band gap is significantly less than in the upper half of the band gap. For example, $N_{SS} \approx 9.5 \times 10^9$ cm^{-2} at $\psi_S = 0.08$ eV and $N_{SS} \approx 1.9 \times 10^{10}$ cm^{-2} at $\psi_S = 0.48$ eV.

Hence, it follows that the densities of surface states in the lower half of the band gap have low values and change insignificantly in magnitude at an energy distance of ~0.48 eV from the middle of the band gap. It should be noted here that, in both the upper half and the lower half of the band gap, there are effective densities of surface states with charged states, which naturally does not include neutral surface states of the N_a^0 type (neutral acceptor surface states).

The experimental results presented above confirm the fact that we obtained the n-CdS–p-Si heterojunction with a relatively low density of surface states, even though the lattice constant of cadmium sulfide and silicon differ by more than 7%. The obtained experimental results are understandable if we take into account that, in the heterojunction, there is an intermediate layer that smoothes the difference in the lattice constants of cadmium sulfide and silicon. Such intermediate layers can be solid solutions of these semiconductors or thin oxide layers that exist on the surface of silicon (SiO_2) or arise (CdO_x and SO_x) during the formation of the n-CdS–p-Si heteropair. However, the determination of the composition of the intermediate layer is the subject to further investigation.

Thus, the results obtained from the capacitance–voltage characteristic demonstrate that the structure under investigation behaves as an MIS structure, in which the main potential barrier is created in the n-CdS subsurface layer at the interface of the n-CdS–p-Si heterojunction. These data also demonstrate that one of the reasons for the high concentrations of nonequilibrium electrons in the high-resistivity base (n-CdS) in the forward direction of the current is a relatively low density of surface states in the lower half of the band gap of silicon. This circumstance can be explained by the fact that, in the forward direction of the current, nonequilibrium charge carriers interact with the surface states N_{SS} located in the lower half of the band gap, whereas in the opposite direction, they interact with the surface states located in the upper half of the band gap of silicon. Based on these data, we constructed the band diagram of the M(In)–n-CdS–p-Si–M(In) structure (Fig. 8).

The band diagram of the M(In)–n-CdS–p-Si–M(In) structure (Fig. 8) indicates that the forward and reverse currents are limited by the electrical resistance of the space-charge layer at the interface of the n-CdS–p-Si heterojunction. This space charge consists of positively charged immobile donor centers and mobile holes and is located in the n-CdS subsurface layer, because the concentration of holes in p-Si is ten orders of magnitude greater than the concentration of electrons in the n-CdS layer. In this structure, the contact between metallic indium and n-CdS is also provided by the contact potential difference $V_c = 1.1$ eV.

However, in this case, an enriched space charge layer arises on the n-CdS surface, because the work function of the metal (indium) is less than the work function of the semiconductor (n-CdS) (Fig. 8). Therefore, the external potential applied to the structure, including the contact potential difference, falls predominantly on the space charge layer formed between p-Si and n-CdS. It should be noted that, in this case, the surface states N_{SS} at the interface between the contacting semiconductors of cadmium sulfide and silicon can affect the height of the potential barrier, the nature of which is determined both by the difference in the parameters of the crystal lattices of the heteropair and by the technological conditions used in the fabrication of the heterojunction.

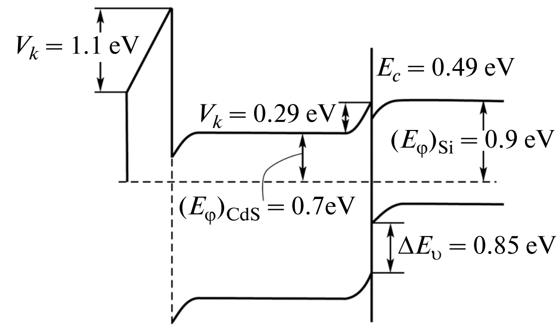

Fig. 8. Energy band diagram of the M(In)–n-CdS–p-Si–M(In) structure.

3.3. Forward Current–Voltage Characteristic

It is known that the injection and accumulation properties of potential barriers determine the current–voltage characteristics of the structure. Therefore, we investigated the forward current–voltage characteristic of the structure in the dark, which is shown in Fig. 1 on a semilogarithmic scale. The analysis of the forward current–voltage characteristic of the M(In)–n-CdS–p-Si–M(In) structure revealed that, at room temperature, it consists of four sections.

The first, second, and fourth sections of the forward current–voltage characteristic are described by the exponential dependence of the electric current on the voltage and can be represented by the following analytical expression:

$$I = I_0[\exp(qV/ckT) - 1], \tag{3}$$

where c is the exponent, I_0 is the pre-exponential factor, q is the electron charge, k is the Boltzmann constant, T is the temperature in degrees Kelvin, and V is the bias voltage. It should be noted that the parameters c and I_0 have different values for each section of the current–voltage characteristic. The third section of the current–voltage characteristic is described by a sublinear dependence of the electric current on the voltage.

Let us now analyze these sections of the forward current–voltage characteristic. The first section of the current–voltage characteristic is observed at current densities $I \approx 10^{-7}$–4×10^{-6} A/cm^{-2} for the exponent $c_1 = 1.04$ and the pre-exponential factor $I_{01} = 1.3 \times 10^{-8}$ A/cm^2 (see inset in Fig. 1). Formula (3) has these values of c and I_0 when thermionic emission currents flow through the structure [14]. Thermionic emission currents flow through the structures with the Schottky barrier and in the MIS structures. The thermionic emission current is described according to the following formula [18]:

$$I = AT^2 e^{-\frac{V_D}{kT}}\left(e^{\frac{eV}{ckT}} - 1\right) = I_{01}\left(e^{\frac{eV}{ckT}} - 1\right). \tag{4}$$

Here,

$$I_{01} = AT^2 e^{-\frac{V_D}{kT}}, \tag{5}$$

where A is the Richardson constant, $A = 12 \times 10^5$ A/(m^2 K^2); V_D is the height of the potential barrier; and V is the bias voltage.

Using the experimental value $I_{01} = 1.3 \times 10^{-8}$ A/cm^2, which was determined from the first section of the current–voltage characteristic according to expression (5), we found the potential barrier height $V_D = 0.86 \pm 0.02$ eV, which agrees well with the potential barrier determined from the current–voltage characteristic (see Subsection 3.2). Thus, it was shown that, in the first section of the current–voltage characteristic, the current flows according to thermionic emission mechanism. In this case, the current in the M(In)–n-CdS–p-Si–M(In) structure is determined by thermionic emission of electrons from M(In) into n-CdS (Fig. 8).

In the second section of the current–voltage characteristic in the range of current densities $I = 1.8 \times 10^{-6}$–4×10^{-5} A/cm^2, the parameters c and I_0 significantly increase and become equal to 3.6 and 5.4×10^{-8} A/cm^2, respectively (see inset in Fig. 1). The performed analysis demonstrated that there is an injection of charge carriers from the M(In)–n-CdS contact into the quasi-neutral part of the base (n-CdS), and its resistance plays an important role in determining the current–voltage characteristic. In this case, holes are not injected from the n-CdS–p-Si heterojunction into the base, as was shown in [17]. This conclusion is valid only for ideal heterojunctions. In real heterojunctions, there exist surface states at the interface of the semiconductors, and they can be recombination centers or centers for tunneling of holes. Nevertheless, we believe that the current in the structure is predominantly determined by electron fluxes coming from the M(In)–n-CdS contact. The analysis of the second

section of the current–voltage characteristic shows that diffusion currents generated by minority nonequilibrium charge carriers (holes) flow in the base. These currents come from the opposite n-CdS–p-Si contact in order to ensure the electroneutrality of injecting electrons. From the literature, it is known that, if the effect of accumulation is insignificant, among the large diversity of current–voltage characteristics in the diffusion mode, there remain only the dependences $I \sim \exp(qV/kT)$ and $I \sim \exp(qV/ckT)$, which were obtained for the first time by Shockley [19] and Stafeev [20] for p–n diode structures with an ohmic contact and a significant resistance of the base.

The expression obtained for the diffusion current by Stafeev has the following form [20]:

$$I = I_{02}\exp(qV/ckT), \tag{6}$$

where

$$c = (2b + \cosh(w/L) + 1)/(b + 1), \tag{7}$$

$$I_c = (kT/q)(b\cosh(w/L))/[2(b + 1)L\rho\tan(w/2L)], \tag{8}$$

$b = \mu_n/\mu_p$ is the ratio of the electron and hole mobilities, w is the thickness of the base, ρ is the electrical resistivity of the base, I_{02} is the pre-exponential factor, and L is the minority carrier diffusion length.

Substituting the experimental value $c = 3.6$ into formula (7), we find that $L = 0.48$ μm, $\mu\tau = 8.8 \times 10^{-8}$ cm^2/V (the product of the mobility by the lifetime of holes) for the parameters $b = 38$ [9] and $w = 2$ μm. It should be noted that the obtained data for the diffusion length L relate to the bipolar diffusion length, because the base of the structure is a high-resistivity compensated material. Therefore, nonequilibrium charge carriers diffuse in the form of a plasma; i.e., electron–hole pairs move together, and their direction corresponds to the direction of the motion of minority charge carriers, namely, holes. The plasma of electron–hole pairs diffuse like uncharged particles, in which the mobility and diffusion coefficient remain unchanged. The validity of this mechanism of current flow is confirmed by the following estimate. We obtained the relaxation curves in the absence of a bias voltage. The relaxation time constants $\tau = 3.5 \times 10^{-8}$ and 1.2×10^{-7} s were determined from the increasing and decreasing relaxation curves, respectively. Further, assuming that the first relaxation time constant is the hole lifetime, from the experimental value of the bipolar diffusion length L, we determined the bipolar diffusion coefficient $D \approx 5.8 \times 10^{-2}$ cm^2/s for values of $L = 0.48$ μm and $\tau = 3.5 \times 10^{-8}$ s. The bipolar diffusion mobility $\mu_d \sim 2.5$ cm^2/(V s) found from the coefficient $D = (kT/q)$ is in good agreement with the data available in the literature ($\mu_p = 7$–8 cm^2/(V s)) [9], if we take into account that the base of the structure under investigation is a polycrystalline material. Then, using the obtained value of the bipolar diffusion coefficient $D \approx 5.8 \times 10^{-2}$ cm^2/s and formula [18] $D = (D_p\sigma_n + D_n\sigma_p)/(\sigma_p + \sigma_n)$, where σ_p and σ_n are the hole and electron conductivities of the base, respectively, we evaluated the ratio of the electron conductivity to the hole conductivity of the base $\sigma_n/\sigma_p \approx 20$, when the electron mobility exceeds the hole mobility by a factor of 40, i.e., $\mu_n = 40\mu_p$ [9]. For this ratio of the electron and hole conductivities in the base, the bipolar drift mobility $\mu_E \approx \mu_d$ according to the estimate made from the formula [18] $\mu_a = (\mu_n\sigma_p - \mu_p\sigma_n)/(\sigma_p + \sigma_n)$. For this value of the bipolar drift mobility of holes, we obtained the bipolar drift velocity of holes $v_a \approx 2.5 \times 10^2$ cm s^{-1} and the bipolar drift length $L_{dr} \approx 6 \times 10^{-5}$ cm for the parameters $\mu_a = 2.5$ cm^2/(V s), $w \approx 2$ μm, $\tau = \sim 10^{-8}$ s, and $V = 0.5$ V. Hence, it follows that the values of L and L_{dr} are almost identical; therefore, in the second section of the forward current–voltage characteristic, the dependence of the current on the voltage is described by the diffusion mechanism [13].

The quantity I_{02} is approximately equal to the current at which the conductivity of the base region is twofold increased by the injection; i.e., the equilibrium conductivity becomes equal to the nonequilibrium conductivity of the base, followed by the transition to high levels of injection. Therefore, assuming that $I_{02} = 5.4 \times 10^{-8}$ A/cm^2 corresponds to the initial voltage of the second section of the current–voltage characteristic (0.1 V), we find the electrical resistivity of the base $\rho = 1.5 \times 10^{10}$ Ω cm.

The electrical resistivity of the base ρ thus determined is the lower limit, whereas the direct measurement of the resistivity of the film shows that $\rho \approx 2.3 \times 10^{10}$ Ω cm.

It can be seen from Fig. 1 that, between the second and third sections of the current–voltage characteristic, there is a section with the curvature. According to the data available in the literature [12, 13], a sublinear section of the current–voltage characteristic is observed when the diffusion and drift fluxes of nonequilibrium charge carriers are directed toward each other. As was mentioned above, in the forward direction of the current, the electroneutrality of injected electrons in the high-resistivity base of the M(In)–n-CdS–p-Si–M(In) structure is provided by an equal amount of holes coming from the opposite contact. Most likely, in order to realize a sublinear section of the current–voltage characteristic, the counter diffusion and drift currents should have almost the same value. In the structure under consideration, the bipolar diffusion current directed to the n-CdS–p-Si heterojunction and the bipolar drift currents directed to the n-CdS–M(In) contact satisfy the above condition at bias voltages of 3–8 V, so that, in the experiment, there appears a sublinear section of the current–voltage characteristic. If the modulation of filling of deep centers plays a decisive role in the bipolar drift velocity

of nonequilibrium charge carriers, the current–voltage characteristic in sublinear section is described by the following analytical expression [12, 13]:

$$V = V_0 \exp(aIw), \tag{9}$$

where

$$a = (1/2)qD_pN_t. \tag{10}$$

In expression (9), V_0 is the pre-exponential factor $V_0 = \frac{D_{\text{eff}}}{\mu_p}\frac{b+1}{b(b\gamma+b+1)}\frac{p_{sb}^2}{N_tp(w)}$, where D_{eff} is the bipolar diffusion coefficient, $\gamma = \frac{N_t}{p_{1t}}$ is the trapping factor, p_{1t} is the static Shockley–Read factor, p_{sb} is the concentration of nonequilibrium holes around the cathode (near the *M*(In)–*n*-CdS) contact), $p(w)$ is the concentration of nonequilibrium holes around the anode (near the *n*-CdS–*p*-Si contact). In formula (10), D_p is the hole diffusion coefficient, N_t is the concentration of trapping levels, and I is the current density.

Using expressions (9) and (10), we determined the concentration of deep trapping centers $N_t = 2 \times 10^{10}$ cm^{-3} for the parameters $\mu_p \approx 2.5$ cm^2/(V s) and $w = 2$ μm. In this case, the expressions for the bipolar drift velocity and the diffusion coefficient are simplified as follows:

$$v_a \approx aID_a, \quad D_a \approx D_p. \tag{11}$$

According to the estimation performed using formula (11), we obtained the bipolar drift velocity $v_a \approx 6.5 \times 10^4$ cm/s for the parameters $a \approx 10^8$ cm^{-1} A^{-1}, $I \approx 1.15 \times 10^{-4}$ A cm^{-2}, and $D_a \approx 5.8 \times 10^{-2}$ cm^2/s (as in the second section of the current–voltage characteristic). At this bipolar drift velocity of holes, the electron–hole plasma travels a distance equal to $L_{\text{dr}} \approx 6.5 \times 10^{-4}$ cm for the lifetime of nonequilibrium charge carriers (~10^{-8} s), which exceeds the bipolar diffusion length by a factor of more than 20. This suggests a modulation in the bipolar drift velocity of nonequilibrium charge carriers, and the contribution from the bipolar drift current to the total current becomes significant.

As was noted above, the fourth section of the current–voltage characteristic is described by the exponential dependence $I = I_{04}\exp(qV/c_4kT)$, where $c_4 = 68$ and $I_{04} = 1.9 \times 10^{-7}$ A/cm^2. Substituting these experimental values into formulas (7) and (8), we determine the ratio of the thickness of the base to the diffusion length of holes $w/L = 8.5$ and $L = 0.24$ μm, as well as the electrical resistivity of the base $\rho = 1.9 \times 10^7$ Ω cm. The parameters L and ρ estimated from the fourth section of the current–voltage characteristic differ significantly from those calculated from the second section of the current–voltage characteristic. The difference between these values can be explained by a change in the properties of the base with an increase in the current density in the structure. After the sublinear section of the current–voltage characteristic, the recharging of highly compensated recombination centers leads to a decrease in the lifetime of minority carriers, namely, holes. The structure acquires the properties of "long" diodes [21], in which the current is predominantly determined by the drift mechanism. In order to confirm this assumption, we determined the bipolar diffusion and drift mobilities from the fourth section of the current–voltage characteristic. The experiments demonstrated that the bipolar diffusion length in the fourth section of the forward current–voltage characteristic is two times less than the value of L in the second section of the current–voltage characteristic and is equal to 0.24 μm. In this case, the product $\mu\tau$ decreases by a factor of four. Further, assuming that the mobility and lifetime of the plasma of electron–hole pairs equally decrease by a factor of two, from the expression $L = (D\tau)^{0.5}$, we find that $D_a = 3.3 \times 10^{-1}$ cm^2 s^{-1} for the parameters $L = 0.24$ μm and $\tau = 1.75 \times 10^{-8}$ s. Since $D_a = (kT/q)\mu_D$, we find that the mobility of the bipolar diffusion of free carriers $\mu_D = 12.5$ cm^2/(V s). The bipolar drift mobility of free carriers was determined as follows. It was assumed that, in this section of the current–voltage characteristic, the determining current in the structure is the drift current. Therefore, from the values of the voltage and current at the end of the fourth section of the current–voltage characteristic ($V = 20$ V, $I = 0.18$ A/cm^2), we determined the electrical resistivity of the base of the structure. Next, assuming that all the hole trapping centers ($N_t = 2 \times 10^{10}$ cm^{-3}), which play a decisive role in the modulation of the bipolar drift velocity in the sublinear section of the current–voltage characteristic, are filled, we find that the concentration of the electron–hole plasma is no less than 10^{11} cm^{-3}, which is significantly higher than the concentration of the trapping centers. Then, using the formula $R = \rho w/S$, where $w \approx 2$ μm (thickness of the base), ρ is the electrical resistivity of the base, and $S = 0.1$ cm^2 is the active surface area of the structure, we determined the bipolar drift mobility $\mu_a = {\sim}112$ cm^2/(V s). It is known that a significant part of the applied potential in the injection diodes drops across the base of the structure. Therefore, for simplicity, it is assumed that the potential $V = 20$ V applied to the structure is equally distributed among the *M*(In)–*n*-CdS injecting contact and the base (*n*-CdS). In this case, we have the bipolar drift velocity of holes $v_a \approx 5.6 \times 10^6$ cm/s. For this bipolar drift velocity, we obtain the bipolar drift length of holes $L_{\text{dr}} \approx 5.6 \times 10^{-2}$ cm for the parameter $\tau \approx 10^{-8}$ s (the lifetime of the electron–hole plasma), which is more than three orders of magnitude greater than the bipolar diffusion length ($L = 0.24$ μm). The estimations performed above demonstrate the dynamics of increase in the bipolar drift velocity, which completely

confirms that, in the fourth section of the current–voltage characteristic, the drift mechanism dominates.

The fourth section of the current–voltage characteristic is also fairly well described by the power law $I \sim V^2$. At sufficiently high levels of injection, the concentration of nonequilibrium charge carriers for the M(In)–n-CdS junction increases substantially. Consequently, even in the asymmetric junction, the second component of the current, i.e., the drift current, begins to play a significant role [17]. In this case, the charge carrier drift in an electric field begins to play a decisive role even at the boundary of the space charge layer. The electrical conductivity of the base layer increases more slowly as compared to the increase in the current, and the current–voltage characteristic is described by the power law [17]

$$I = (9/8)q(n_0 - p_0)\mu_n\mu_p\tau(V^2/w^3)S, \quad (12)$$

where n_0 and p_0 are the equilibrium concentrations of electrons and holes, respectively; μ_n and μ_p are the electron and hole mobilities, respectively; and τ is the lifetime of the electron–hole plasma.

Further, according to formula (12), we calculated the product $\mu_n\mu_p \approx 4 \times 10^7$ (cm^2 V^{-1} s^{-1})^2 for the parameters $\rho \approx 2 \times 10^{10}$ Ω cm, $n_0 \approx 10^6$ cm^{-3}, and μ_n = 289 cm^2 V^{-1} s^{-1} [9], the current $I = 0.18$ A cm^{-2}, and the voltage $V = 20$ V. The obtained value of the product $\mu_n\mu_p$ is four orders of magnitude greater than that found in [22]. This difference is obtained for the electron mobility $\mu_n = 289$ cm^2 V^{-1} s^{-1} and the hole mobility $\mu_p = 8$ cm^2 V^{-1} s^{-1}, i.e., as in the case of CdS single crystals [9]. Moreover, the above estimate shows that there is a modulation of the conductivity of the base, where the main role is played by a rapid increase in the bipolar drift mobility of nonequilibrium charge carriers with the current. This is explained by the fact that the bipolar mobility of the electron–hole plasma, according to [22],

$$\mu = \frac{n - p\frac{dn}{dp}}{n\mu_n + p\mu_p}\mu_n\mu_p, \quad (13)$$

in the numerator, has the quantity that depends on the difference in the concentrations of charge carriers. Probably, in the fourth section of the current–voltage characteristic, the numerator of expression (13) changes, which leads to a sharp increase in the bipolar mobility of the electron–hole plasma. The reason for this behavior can be trapping levels for holes, which actively manifest themselves at the same current densities at which the fourth section of the current–voltage characteristic appears.

The investigations of the light current–voltage characteristic for different levels of illumination by the white light and for different laser irradiation powers demonstrated that the current–voltage characteristic are identical in shape and have the same regularities of change in the current as a function of the bias voltage (Fig. 3). Moreover, the maximum values of the integrated and spectral sensitivities are observed in the fourth section of the current–voltage characteristic (Table 1). From the data presented in Table 1, it follows that the highest value of the amplification of the primary photocurrent is observed at low levels of illumination by the white light, In this case, the amplification of the primary photocurrent increases with an increase in the bias voltage. For example, for the illumination by the white light with an illuminance E = 0.05 lx and at an applied forward bias voltage $V = 20$ V, we have the integrated sensitivity $S_{\text{int}} = 4.06 \times 10^4$ A/lm (4.47×10^6 A/W), which decreases with an increase in the illumination level and with a decrease in the bias voltage. It can also be seen from Table 1 that, under the laser irradiation with $\lambda = 0.625$ μm, the spectral sensitivity S_λ is significantly less than the integrated sensitivity S_{int} for the same values of the incident radiation powers and the same values of the bias voltages. For example, for comparison, the integrated sensitivity $S_{\text{int}} \approx 3.4 \times 10^5$ A/W upon illumination by the white light with $E = 1$ lx (9.1×10^{-7} W/cm^2) and the spectral sensitivity $S_\lambda = 5.04 \times 10^4$ A/W at a laser irradiation power of ~7×10^{-7} A/W and a bias voltage $V = 20$ V. Hence, it follows that the amplification of the primary photocurrent occurs according to two mechanisms: the "positive feedback" mechanism [23] and the parametric mechanisms [22, 24]. It should be noted that the base of the structure under investigation is a high-resistivity highly compensated semiconductor material. Therefore, the base can include several deep trapping levels, the modulation of filling for which occurs under illumination by the white light.

3.4. Reverse Current–Voltage Characteristic

For convenience of the analysis, the reverse current–voltage characteristic of the structure is presented in Fig. 1 for positive values of current. The analysis demonstrates that, in the range of current densities $I \approx 1.3 \times 10^{-9}$–$1.1 \times 10^{-8}$ A/cm^2, thermionic currents flow through the structure, because, in this region, the current exponentially depends on the voltage with the ideality factor $c \approx 1.05$ and the pre-exponential factor $I_0 = 2.9 \times 10^{-9}$ A/cm^2. Using the value of $I_0 = 2.9 \times 10^{-9}$ A/cm^2, according to formula (5), we obtained the height of the potential barrier $V_D = 0.98 \pm 0.02$ eV, which is approximately equal to the value determined from the forward current–voltage characteristic. This is not surprising, because, in both cases, we determined the same height of the potential barrier, and only the direction of the current in the studied structure. The emission of electrons occurs from cadmium sulfide into the metal (indium).

In the range of current densities $I \approx 1.3 \times 10^{-8}$–$5.2 \times 10^{-7}$ A/cm^2, the current–voltage characteristic is described by the exponential dependence $I = I_{02}\exp(qV/ckT)$ with the exponent $c_2 = 5.2$ and the pre-exponential factor $I_{02} = 1.8 \times 10^{-8}$ A/cm^2. This section differs from the corresponding section of the forward current–voltage characteristic. It is characterized by somewhat different values of the exponent c and the pre-exponential factor I_0. Substituting the experimental value $c_2 = 5.2$ determined from the second section of the current–voltage characteristic into formula (4), we obtained the diffusion length of the plasma of nonequilibrium charge carriers $L = 0.27$ μm and the bipolar diffusion coefficient $D = 7.3 \times 10^{-2}$ cm^2 s^{-1} for the relaxation time constant $\tau = {\sim}10^{-8}$ s. The estimation was performed for the base thickness $w = 1.5$ μm, because, in this case, we took into account the thickness of the space charge of the n-CdS–p-Si heterojunction, which is equal to ~0.5 μm at the thermodynamic equilibrium. Then, we performed the same estimation as in the case of the forward the current–voltage characteristic (see Subsection 3.3). The results obtained were used to determine the bipolar diffusion and drift mobilities of nonequilibrium charge carriers, which are equal to 2.8 and 3.9 cm^2 V^{-1} s^{-1}, respectively, and have nearly identical values. This means that the charge transfer occurs with the participation of both types of nonequilibrium charge carriers, and the flow of the diffusion current is accompanied by the flow of the drift current.

A further increase in the bias voltage leads to an increase in the concentration of electrons injected from the n-CdS–p-Si heterojunction. Therefore, the concentration of holes should increase by the same value in order to provide the electrical neutrality. The drift of the bipolar current also increases due to the increase in the bipolar drift velocity. An increase in the bipolar drift velocity $v_a(I)$ with an increase in the current density can lead to the formation of a relative depletion layer near the accumulation contact (i.e., near the n-CdS–p-Si heterojunction) of the n-base, in which the concentration decreases with an increase in the current density [12, 13]. Such a local decrease in the concentration $p(x)$ results in a rapid increase in the electrical resistivity of the n-base. The formation of the relative depletion region is caused by the “displacement” of the steep diffusion front of the function $p(x)$ due to an increase in the bipolar drift of free charge carriers with an increase in the current density, which deforms the profile of their distribution in the n-base. An increase of this deformation leads to an increase in the slope of the function $p(x)$ and to the corresponding enhancement of the counter diffusion transport of charge carriers. The competition between the diffusion and drift fluxes provides both the mutual compensation of their changes with increasing current and the formation of the internal feedback in voltage and a sublinear section of the current–voltage characteristic, which has the following analytical expression [13]:

$$V \approx V_0\exp(v_a w/D_a) = V_0\exp(Iaw)$$

(where w is the base thickness and I is the current density), when the modulation of the bipolar velocity results in an exponential increase in the bias voltage V applied to the base as a function of the current I. Consequently, the properties of the n-base and the accumulation contact play an important role in the realization of the diffusion/drift mode. In this case, the concentration at the accumulation contact and even the character of its dependence on the current are less significant, whereas more important is the profile of the distribution of nonequilibrium charge carriers in the n-base, which create the counter directions of the bipolar diffusion and drift fluxes. Moreover, the accumulation contact should be ideal and almost opaque for minority carriers. In the structure under investigation, the n-CdS–p-Si heterojunction should be such contact for holes in the n-base.

The appearance of a sublinear section in the reverse current–voltage characteristic over a wide range of bias voltages ($V \approx 10$–60 V) indicates that the region of the mutual compensation of the drift and diffusion fluxes of nonequilibrium charge carriers in the M(In)–n-CdS–p-Si–M(In) structure is wide enough. This result also suggests that the n-CdS–p-Si heterojunction, which is an accumulation contact, is almost opaque for holes, and in this heterojunction, the acceptor surface states are very small, so that there are no leakage currents.

This is indicated by the fact that, as the reverse bias voltage increases by almost one order of magnitude, i.e., from 8 to 60 V, the current in the structure changes only slightly (by only ~4×10^{-7} μA/cm^2, i.e., by ~10%). Since the dynamics of increase in the bipolar drift velocity v_a with increasing current plays the main role in the implementation of the aforementioned physical processes, we estimated the bipolar drift velocity v_a in different sections of the current–voltage characteristic. First, we estimate the bipolar drift velocity in the sublinear section of the current–voltage characteristic. For this purpose, we assume that the bipolar drift velocity v_a is determined exclusively by the modulation of filling of deep impurities in the form of trapping centers for holes. The bipolar drift velocity is determined by the expression [13]

$$v_a = (I/q)\mu_n\mu_p N_t/[(\mu_n + \mu_p)^2(p^*)^2], \qquad (14)$$

where $p^* = p_{1t} + \mu_n N_t/(\mu_n + \mu_p)$. Under the condition of the prevailing influence of the modulation of depth trapping centers, we have the trapping factor $\gamma = N_t/p_{1t} \gg 1$, and at $p < p^*$, the expressions for the diffusion coefficient and the bipolar drift velocity are simplified: $D_a \approx D_p$ and $v_a \approx aID_a$, where $a = 1/2qD_nN_t$ is the parameter dependent only on the concentration of deep trapping centers N_t.

Table 2. Photocurrent I_{Ph}, integrated sensitivity S_{int}, and spectral sensitivity S_λ as functions of the bias voltage V

White light					Laser irradiation		
E, lx	V, V	I_{Ph}, μA/cm^2	S_{int}, A/lm	S_{int}, A/W	P, μW/cm^2	I_{Ph}, μA/cm^2	S_λ, A/W
0.1	5	3.65	0.365	40.1	10	13.1	1.31
	10	4.3	0.43	47.36		18.83	1.883
	60	6.9	0.6916	76		32.8	2.28

From the sublinear section of the current–voltage characteristic, we find that the parameter $a = (2/1.5) \times 10^{11}$ cm^{-1} A^{-1} and then estimate the bipolar drift velocity of nonequilibrium charge carriers $v_a \approx 2 \times 10^6$ cm s^{-1} for the parameters $I = 2 \times 10^{-6}$ A/cm^2 and $D_a \approx 7.3$ cm^2 s^{-1} (as in the second section of the current–voltage characteristic). The estimated bipolar drift velocity of nonequilibrium charge carriers is more than three orders of magnitude greater than the value of $v_a \approx 1.2 \times 10^3$ cm s^{-1} determined from the second section of the current–voltage characteristic. Hence, it follows that the mechanism of increase in the bipolar drift velocity is the modulation of filling of deep trapping centers for holes, which leads to an increase in the electrical resistivity of the base, and the electric field strength in it increases. Moreover, the performed evaluation shows the dynamics of increase in the bipolar drift velocity of nonequilibrium charge carriers with an increase in the current. The existence of the diffusion and drift flows directed toward each other creates a strong inhomogeneity of the distribution $p(x)$. This inhomogeneity determines high values of the hole concentration gradient (dp/dx), which allow us to ignore the contribution from the generation–recombination processes to the relaxation of the perturbed electron–hole plasma:

$$(v_a\tau_p/L) \gg (p - p_n)/\tau_p, \quad (15)$$

where $L = (D_a\tau_p)^{0.5}$ is the bipolar diffusion length and $L_{\text{dr}} = v_a\tau_p$ is the bipolar drift length for holes.

Inequality (15) means that the generation–recombination processes can be ignored for sufficiently large values of the bipolar drift lengths for holes ($L_{\text{dr}} \gg L$). In the sublinear section of the reverse current–voltage characteristic, we have the bipolar drift length $L_{\text{dr}} = 2 \times 10^{-2}$ cm for the parameters $v_a = 2 \times 10^6$ cm s^{-1} and $\tau_p = 10^{-8}$ s and the carrier diffusion length $L = 2.8 \times 10^{-5}$ cm for the parameters $D_a \approx 7.3 \times 10^{-2}$ cm^2 s^{-1} and $\tau_p = 10^{-8}$ s. From this estimate, it follows that, in the sublinear section of the current–voltage characteristic, inequality (15) holds true because the bipolar drift length for holes is three orders of magnitude greater than the bipolar diffusion length. Therefore, we can ignore the generation–recombination processes in the relaxation of perturbations of the electron–hole plasma. It is entirely determined by the bipolar diffusion and drift processes. For comparison, we note that, in the second section of the current–voltage characteristic, the values of L and L_{dr} are equal to $L = 2.7 \times 10^{-5}$ cm and $L_{\text{dr}} = 1.4 \times 10^{-5}$ cm; i.e., they differ by a factor of approximately 2, but the diffusion current was found to be decisive because there is a concentration gradient of nonequilibrium charge carriers.

It was of interest to analyze the behavior of the sublinear section of the current–voltage characteristic under illumination by the white light and under laser irradiation. Therefore, we investigated the light current–voltage characteristics under illumination at $E = 0.1$ lx and under laser irradiation with a wavelength $\lambda = 0.625$ μm and a power $P = 10$ μW/cm^2, which are shown in Fig. 3. It can be seen from this figure that the light and dark current–voltage characteristics have the same regularities and differ only in the magnitude of the current. The light and dark current–voltage characteristics measured under laser irradiation differ from each other by more than 1.5 orders of magnitude, whereas the corresponding characteristics measured under illumination by the white light differ in the magnitude of the current by a factor of 4. Upon laser irradiation, we have the spectral sensitivity $S_\lambda \approx 3.3$ A/W at the bias voltage $V = 60$ V. Upon illumination by the white light with $E = 0.1$ lx and $V = 60$ V, we have the integrated sensitivity $S_{\text{int}} \approx 0.6916$ A/lm (~76 A/W). These results demonstrate (Table 2) that, under laser irradiation, in the sublinear section of the current–voltage characteristic, there is an amplification of the primary photocurrent, which is more than 6 times higher than the photosensitivity of an ideal photodetector at a given wavelength of electromagnetic radiation ($S_\lambda \approx 0.5$ A/W at the wavelength $\lambda = 0.625$ μm) [25]. Under illumination by the white light with the illuminance $E = 0.1$ lx, the integrated sensitivity S_{int} is almost 20 times higher than the spectral sensitivity of the ideal photodetector at the wavelength $\lambda = 0.625$ μm. The spectral dependence of the photosensitivity for an ideal photodetector, which is constructed according to the formula $S_\lambda = \frac{e}{hc}\lambda\eta_\lambda$ [25] (where e is the electron charge, h is the Planck's constant, c is the speed of light, and η_λ is the quantum yield of the internal photoeffect), is shown in Fig. 2 for the cases where the bias voltage is applied in the forward direction (curve *4* in Fig. 2a) and in the reverse direction (curve *5*

in Fig. 2b) of the current. Also, we estimated the ambipolar drift velocity of charge carriers v_a under illumination by the white light and under laser irradiation. For this purpose, using formula (9), we determined the value of the parameter a upon illumination by the white light and under laser irradiation. It was found that the parameter a has almost the same values (~10^{11} cm^{-1} A^{-1}) under illumination by the white light, laser irradiation, and in the dark. As can seen from formula (11), the ambipolar drift velocity depends linearly on the current density. Hence, it follows that the velocity v_a increases so many times, how many times the magnitude of the photocurrent increases in comparison with the dark current (of course, at a constant value of the bipolar diffusion coefficient). Thus, we have $v_a \approx 10^8$ cm s^{-1} under laser irradiation with a wavelength $\lambda = 0.625$ μm and a power of $P = 10$ μW/cm^2, whereas under illumination by the white light at an illuminance $E = 0.1$ lx, we obtain $v_a \approx 4 \times 10^6$ cm s^{-1}; i.e., they increase so many times, how many times the photocurrents were increased. It should be noted that, in the evaluation, we assumed that the bipolar diffusion coefficient has the same as in the second section: $D_a \approx 7.3$ cm^2 s^{-1}. Thus, it was shown that an increase in the bipolar drift velocity of nonequilibrium charge carriers plays an important role in the amplification of the primary photocurrent in the sublinear section of the current–voltage characteristic.

The aforementioned effect of increase in the electrical resistivity of the base, which was observed over a wide range of bias voltages, can be used in the development of semiconductor devices for various applications (rectifiers with a high rectification ratio, zener diodes, etc.).

4. CONCLUSIONS

We fabricated a photosensitive M(In)–n-CdS–p-Si–M(In) structure. This structure at a reverse bias voltage is characterized by an injection of electrons from the narrow-band-gap semiconductor p-Si to the wide-band-gap semiconductor n-CdS. At current densities $I \sim 10^{-8}$–10^{-7} A/cm^2, there is a sign reversal of the photosensitivity in the short-wavelength and long-wavelength regions of the spectrum. With an increase in the bias voltage, the sign-reversal point of the photosensitivity in the short-wavelength region of the electromagnetic radiation spectrum shifts toward shorter wavelengths, whereas the sign-reversal point of the photosensitivity in the long-wavelength region of the spectrum, on the contrary, shifts towards longer wavelengths. The mutual compensation of the counter drift and diffusion current fluxes at current densities of the order of ~10^{-6} A/cm^2 leads to the appearance of a sublinear section in the reverse current–voltage characteristic over a wide range of bias voltages. An increase in the bias voltage in the forward direction of the current near the M(In)–n-CdS junction results in the accumulation of holes.

It was found that the n-CdS–p-Si heterojunction has a low density of surface states at the interface. This is indicated by a high rectification ratio of the M(In)–n-CdS–p-Si–M(In) structure, as well as by the appearance of a sublinear section in the reverse current–voltage characteristic over a wide range of bias voltages. It was shown that light and dark current–voltage characteristics of the structure have the same specific features of the change in the electric current as a function of the voltage. It was found that an increase in the current density changes the properties of the base structure, which leads to a change in the minority carrier diffusion length and the charge transfer mechanism in the studied structure. It was shown that, with an increase in the current density, the bipolar drift velocity of nonequilibrium charge carriers increases and reaches the highest value in the fourth section of the forward current–voltage characteristic; i.e., the structure is a long diode. It was found that, at current densities $I = 10^{-2}$–5×10^{-4} A/cm^2 in the forward direction of the current, the integrated sensitivity S_{int} and spectral sensitivity S_λ increase significantly. For example, $S_{int} = 2.8 \times 10^4$ A/lm (3×10^6 A/W) at an illuminance level $E = 0.1$ lx and $S_\lambda = 2.3 \times 10^4$ A/W under laser irradiation with a wavelength $\lambda = 625$ nm and a laser irradiation power $P = 10$ μW/cm^2. The obtained values of the integrated and spectral sensitivities are rather high for room temperature. Thus, it can be concluded that the mechanism of amplification of the primary photocurrent at high current densities is predominantly determined by the modulation of the ambipolar drift velocity of nonequilibrium charge carriers.

REFERENCES

1. I. M. Koldaev, V. V. Losev, and B. M. Orlov, Sov. Phys. Semicond. **18** (7), 823 (1984).
2. Sh. A. Mirsagatov and A. K. Uteniyazov, Tech. Phys. Lett. **38** (1), 34 (2012).
3. Sh. A. Mirsagatov, R. R. Kabulov, and M. A. Makhmudov, Semiconductors **47** (6), 825 (2013).
4. Sh. A. Mirsagatov, O. K. Ataboev, and B. N. Zaveryukhin, Fiz. Inzh. Poverkhn. **11** (1), 4 (2013).
5. A. S. Saidov, A. Yu. Leiderman, Sh. N. Usmonov, and K. T. Kholikov, Semiconductors **43** (4), 416 (2009).
6. A. G. Milnes and D. L. Feucht, *Heterojunctions and Metal Semiconductor Junctions* (Academic, London, 1972; Mir, Moscow, 1975).
7. I. B. Sapaev, Dokl. Akad. Nauk Uzb., No. 2, 27 (2013).
8. S. E. Frish, *Optical Measurement Methods* (Leningrad State University, Leningrad, 1976), Part I [in Russian].
9. V. I. Fistul', *Physics and Chemistry of the Solid State* (Metallurgiya, Moscow, 1995), Vols. 1, 2 [in Russian].
10. http://zaz.gendocs.ru/docs/2800/index-1621226.html.

11. A. M. Lampert and P. Mark, *Current Injection in Solids* (Academic, New York, 1970).
12. E. I. Adirovich, P. M. Karageorgii-Alkalaev, and A. Yu. Leiderman, *Double Injection Currents in Semiconductors* (Sovetskoe Radio, Moscow, 1978) [in Russian].
13. P. M. Karageorgii-Alkalaev and A. Yu. Leiderman, *Photosensitivity of Semiconductor Structures with Deep Impurities* (Fan, Tashkent, 1981) [in Russian].
14. S. M. Sze, *Physics of Semiconductor Devices* (Wiley, New York, 1981), Vol. 1.
15. V. G. Georgiu, *Capacitance–Voltage Measurements of Parameters of Semiconductors* (Shtiintsa, Chisinau, 1987), p. 15 [in Russian].
16. Sh. A. Mirsagatov, A. K. Uteniyazov, and A. S. Achilov, Phys. Solid State **54** (9), 1751 (2012).
17. I. M. Vikulin and V. I. Stafeev, *Physics of Semiconductor Devices* (Sovetskoe Radio, Moscow, 1980) [in Russian].
18. P. T. Oreshkin, *Physics of Semiconductors and Dielectrics* (Vysshaya Shkola, Moscow, 1977) [in Russian].
19. W. Shockley, Bell Syst. Tech. J. **28**, 4351 (1949).
20. V. I. Stafeev, Sov. Phys. Tech. Phys. **3**, 1502 (1958).
21. V. V. Osipov and V. I. Stafeev, Sov. Phys. Semicond. **1** (12), 1486 (1967).
22. I. M. Vikulin, Sh. D. Kurmashev, and V. I. Stafeev, Semiconductors **42** (1), 112 (2008).
23. V. I. Stafeev and V. M. Tuchkevich, in *Reports of the 19th Annual Conference on Physics of Electronics*, Massachusetts Institute of Technology, Cambridge, Massachusetts, United States, 1959), Vol. 1, p. 139.
24. I. D. Anisimova, I. M. Vikulin, F. A. Zaitov, Sh. D. Kurmashev, in *Semiconductor Photodetectors*, Ed. by V. I. Stafeev (Radio i Svyaz', Moscow, 1984), p. 101 [in Russian].
25. A. Ambrozyak, *Design and Technology of Semiconductor Photoelectric Devices* (Sovetskoe Radio, Moscow, 1970) [in Russian].

Translated by O. Borovik-Romanova